

The advanced system for the electromagnetic response of high-frequency gravitational waves

Jin Li^{a*}, Lu Zhang^{a†}, Kai Lin^{b‡}, and Hao Wen^{a§}

^a *Department of Physics, Chongqing University, Chongqing 401331, China*

^b *Instituto de Física, Universidade de São Paulo, CP 66318, 05315-970, São Paulo, Brazil*

(Dated: December 7, 2024)

Based on the electromagnetic (EM) response system of high frequency gravitational waves (HFGWs) in GHz band, we mainly discuss the EM response to the relic HFGWs, which are predicted by quintessential and ordinary inflationary models, and the braneworld HFGWs from braneworld scenarios. Both of them would generate detectable transverse perturbative photon fluxes (PPFs) thought to be the signal. Through resetting the magnetic component of Gaussian Beam to be in the standard gaussian form, the signal strength would be enhanced theoretically. Under the typical conditions, the analysis of background noise (background photon fluxes) and shot noise provides the possible transverse detection width for these HFGWs, meanwhile the standard quantum limit estimation proves our detection is possible. Finally according to the principle of maximum signal to noise ratio, we find some optimal system parameters and the relationship between effective width for energy fluxes accumulation and frequency.

Keywords: high frequency gravitational waves; electromagnetic response; transverse detection width; effective width

PACS numbers: 04.30.Nk; 04.25.Nx; 04.30.Db; 04.80.Nn

I. INTRODUCTION

As a crucial topic, the observation of gravitational waves (GWs) has puzzled numerous scientists for so many years. A variety of gravitational waves observation stations appeared successively in the past decades. Most of them pay close attention to the GWs from astronomical objects, and have formed several influential groups. The most representative organizations are LIGO [1, 2] and LISA [3], which are designed for measuring the distortion of space-time caused by GWs through the Michael interferometer principle, and the frequency bands range from 10^{-4} – 10^4 Hz. Meanwhile in the lower frequency band, scientists track the trace of gravitational waves through observing the cosmic microwave background (CMB). Fortunately the signature of Primordial Gravitational Wave from cosmic inflation has been reported recently by BICEP2 at South Pole (i.e. B-mode Polarization on cosmic microwave background)[4]. That implies the wavelength of such primordial GWs is bound to be around cosmological scales (i.e. at very low frequency band) unless it would not leave any singularity on the CMB. Although this achievement need to be further proven (for example, Planck collaboration results[5]-[8]), it can encourage the existing GWs instruments to strive for searching the evidence of GWs in their own frequency band.

Unlike the traditional detectors in the low frequency band, the GWs in microwave band ($\sim 10^8$ Hz– 10^{14} Hz) named as high frequency gravitational waves (HFGWs) carry much more information of the universe evolution. Currently the existence of the HFGWs sources are mainly from relic gravitational waves (GWs) and the GWs in the braneworld scenarios with extra dimensions model[9, 10]. In Quintessential Inflationary Model (QIM)[11]-[15] and ordinary inflationary model with specific inflation parameter [16, 17], the relic GWs in the microwave band (relic HFGWs)($\sim 10^8 - 10^{10}$ Hz) have the dimensionless amplitude around $h \sim 10^{-30} - 10^{-32}$. Using the system for the electromagnetic response of GWs in microwave band (cf.fig.I), the relic HFGWs as the main detectable objects have been studied comprehensively in our previous works[19]-[21]. And the results indicate that the strength of the signal crucially lies in two important factors, i.e., the strength of the longitudinal magnetic component of background EM field and the GW's own dimensionless amplitude. Thus based on the precious design, we plan to choose the standard Gaussian form on longitudinal background magnetic component instead of on the transverse electric component of background EM field. On the other hand, since near the Earth the HFGWs emitted from braneworld black hole with wider frequency band ($10^8 - 10^{14}$ Hz) [10],[22] would be quite powerful with an upper limit of the dimensionless amplitudes

* E-mail: cqjinli1983@cqu.edu.cn

† E-mail: happinesszhanglu@126.com

‡ E-mail: lk314159@hotmail.com

§ E-mail: wenhao@cqu.edu.cn

around $h \sim 10^{-21} - 10^{-22}$. By contrast, the HFGWs from the braneworld might likely arouse much stronger signal than the relic HFGWs. Therefore as the most important aim of this paper, the comparison of signal strength and detection sensitivity from relic HFGWs and braneworld HFGWs will be discussed in detail.

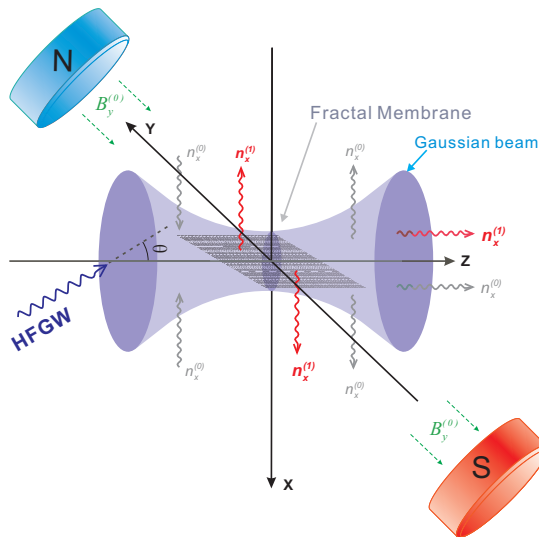


FIG. 1: The advanced configuration of the electromagnetic response scheme basing on the original design[18, 27]

This paper is organized as follows: In section II, the electromagnetic response to the relic HFGWs and the HFGWs from braneworld are calculated, including the discussion of the background EM field. In section III, we take the current possible noise (i.e., background perturbation photons, shot noises) to be considered and estimate the detection sensitivity. Moreover, the Standard Quantum Limit (SQL) is also analysed with the fractal membranes (FM). In section IV according to the signal and noise analysis in above sections, we try to find some optimal parameters to enhance the detection sensitivity. Finally some meaningful remarks and important results are listed in section V. Note in this paper, unless otherwise specified the frequency of the HFGWs is chosen to be 3GHz.

II. ELECTROMAGNETIC RESPONSE TO THE GRAVITATIONAL WAVES IN THE MICROWAVE BAND

As the GWs from celestial bodies, the metric of HFGWs can be written as a small perturbation $h_{\mu\nu}$ to the flat spacetime $\eta_{\mu\nu}$.

$$g_{\mu\nu} = \eta_{\mu\nu} + h_{\mu\nu}, \quad (1)$$

where $h_{\mu\nu}$ represents a small correction to the background metric tensor. Supposing the HFGWs come along the z axis in our coordinate system and considering the metric can be expressed as the following form in Cartesian coordinates:

$$h_{\mu\nu} = \begin{pmatrix} 0 & 0 & 0 & 0 \\ 0 & h_{11} & h_{12} & 0 \\ 0 & h_{21} & h_{22} & 0 \\ 0 & 0 & 0 & 0 \end{pmatrix}, \quad (2)$$

where $h_{11} = -h_{22} = A_{\oplus} \exp[i(k_g z - \omega_g t)]$, $h_{12} = h_{21} = A_{\otimes} \exp[i(k_g z - \omega_g t)]$. Here A_{\oplus} and A_{\otimes} denote the amplitude of the \oplus polarization and \otimes polarization in the laboratory frame respectively. It is worthy to mention that although the expressions of the relic HFGWs and HFGWs predicted by braneworld scenarios are identical, their amplitude and frequency band are different as mentioned in Sec.I and the former is a stochastic signal but the latter is a coherent signal with discrete spectrum [10] from a fixed source. In order to achieve the detection for these two kinds HFGWs from different theoretical models, it is necessary to comprehensively improve the detection sensitivity. Therefore, the comparison of signal from relic HFGWs and HFGWs from braneworld is discussed in the following context.

Generally, due to the fact that the GWs propagation direction is not always parallel to z-axis, it is needed to add the direction term as $\cos\theta$ to above equations, where θ is the intersection angle between the GWs propagation direction

and the positive direction of z -axis (see Fig.I). So

$$h_{\mu\nu} = \begin{pmatrix} 0 & 0 & 0 & 0 \\ 0 & A_{\oplus} \exp[i(k_g z - \omega_g t)] \cos \theta & A_{\otimes} \exp[i(k_g z - \omega_g t)] \cos \theta & 0 \\ 0 & A_{\otimes} \exp[i(k_g z - \omega_g t)] \cos \theta & -A_{\oplus} \exp[i(k_g z - \omega_g t)] \cos \theta & 0 \\ 0 & 0 & 0 & 0 \end{pmatrix}, \quad (3)$$

In Figure I, on y -axis the static magnetic field $\hat{B}_y^{(0)}$ would interact with the incoming HFGWs then generate the perturbative EM signals[19],[23], which can be explained by the electro-dynamical equations in curved spacetime[19],[20],

$$\frac{1}{\sqrt{-g}} \frac{\partial}{\partial x^\nu} (\sqrt{-g} g^{\mu\alpha} g^{\nu\beta} F_{\alpha\beta}) = \mu_0 J^\mu, \quad (4)$$

$$\nabla_\alpha F_{\mu\nu} + \nabla_\nu F_{\alpha\mu} + \nabla_\mu F_{\nu\alpha} = 0, \quad (5)$$

where J^μ indicates the four-dimensional electric current density. For the detector is immersed in vacuum, $J^\mu = 0$. Using the perturbation methods ($F_{\mu\nu} = F_{\mu\nu}^{(0)} + \tilde{F}_{\mu\nu}^{(1)} + O(h^2)$; $F_{\mu\nu}^{(0)}$ and $\tilde{F}_{\mu\nu}^{(1)}$ indicate the background and first-order perturbative EM tensor respectively) and neglecting the second and higher-order perturbation, the first-order perturbative EM fields along positive z -axis can be given by [19],[20],[23]-[25].

$$\tilde{E}_x^{(1)} = \frac{i}{2} A_{\oplus} \hat{B}_y^{(0)} k_g c(z + l_1) \exp[i(k_g z - \omega_g t)] \cos \theta, \quad (6)$$

$$\tilde{B}_y^{(1)} = \frac{i}{2} A_{\oplus} \hat{B}_y^{(0)} k_g (z + l_1) \exp[i(k_g z - \omega_g t)] \cos \theta, \quad (7)$$

$$\tilde{E}_y^{(1)} = -\frac{1}{2} A_{\otimes} \hat{B}_y^{(0)} k_g c(z + l_1) \exp[i(k_g z - \omega_g t)] \cos \theta, \quad (8)$$

$$\tilde{B}_x^{(1)} = \frac{1}{2} A_{\otimes} \hat{B}_y^{(0)} k_g (z + l_1) \exp[i(k_g z - \omega_g t)] \cos \theta, \quad (9)$$

where the superscript $^{(0)}, ^{(1)}$ denote the quantities of background and perturbative field, respectively. And the notation \sim and $\hat{}$ represent the time-dependent and static value. Eq.(8) indicates the perturbative electric field is similar to plane EM, and has accumulative effect in propagation direction. However in the laboratory scale, the accumulative effect in z direction performs not so obvious on the transverse perturbative photon fluxes (PPFs). Certainly, if the background static magnetic field $\hat{B}_y^{(0)}$ is replaced with the background galactic-extragalactic magnetic fields, a significant accumulation effect would emerge [23].

Besides, our EM system also consists of a Gaussian Beam (GB) (see Fig. I) with a fundamental frequency mode[26] propagating along z -axis, which can provide a non-vanishing longitudinal magnetic field component $\tilde{B}_z^{(0)}$. Furthermore due to the equivalent status of electric and magnetic components in EM field and enhancing the transverse perturbative photon flux as possible, we assume the longitudinal magnetic field component with standard Gaussian form as

$$\tilde{B}_z^{(0)} = \frac{\psi_0}{\sqrt{1 + (z/f)^2}} \exp\left(-\frac{r^2}{W^2}\right) \exp\left\{i\left(k_e z - \omega_e t - \arctan \frac{z}{f} + \frac{k_e r^2}{2R} + \delta\right)\right\}. \quad (10)$$

and $\tilde{E}_z^{(0)} = 0$, where $r^2 = x^2 + y^2$, $k_e = 2\pi/\lambda$ (the wave number), $f = \pi W_0^2/\lambda$, $W = W_0[1 + (z/f)^2]^{1/2}$ (W_0 is the minimum spot radius at $z = 0$), $R = z + f^2/z$ (the curvature radius of the wave fronts of the GB at z) and δ is the phase difference between the GB and the resonant HFGWs. ψ_0 is the amplitude of the magnetic element $\tilde{B}_z^{(0)}$, which would be determined by the power of laser source. In order to realize the resonant response between the EM and the HFGWs, it is prerequisite to make sure $k_e = k_g$ as possible. Actually the bandwidth of laser is inevitable, the impact of bandwidth will be discussed in the section IV.

Consequently, the other components of EM field would be determined as follows:

$$\begin{aligned} \int \partial_y \tilde{B}_x^{(0)} dx + \int (\partial_z \tilde{B}_z^{(0)} + \partial_x \tilde{B}_x^{(0)}) dy &= 0, \\ \tilde{B}_y^{(0)} = \int \partial_y \tilde{B}_x^{(0)} dx, \quad \tilde{E}_x^{(0)} &= \frac{ic^2}{\omega_e} \left(\frac{\partial \tilde{B}_z^{(0)}}{\partial y} - \frac{\partial \tilde{B}_y^{(0)}}{\partial z} \right), \\ \tilde{E}_y^{(0)} &= \frac{ic^2}{\omega_e} \left(\frac{\partial \tilde{B}_x^{(0)}}{\partial z} - \frac{\partial \tilde{B}_z^{(0)}}{\partial x} \right). \end{aligned} \quad (11)$$

Unlike pure plane EM waves, the EM components of GB are not completely perpendicular to the propagation direction (z -axis) except for the plane where the beam waist exists. Therefore, considering the $\tilde{E}_y^{(1)}$ from the interaction between HFGWs and the static magnetic field $\hat{B}_y^{(0)}$, it would generate the x -component of the first-order perturbative EM power flux density (i.e., transverse perturbative photon flux $N_x^{(1)}$) by the coupling of $\tilde{E}_y^{(1)}$ and $\tilde{B}_z^{(0)}$. That also can explain why we focus the whole Gaussian mode on $\tilde{B}_z^{(0)}$ to enhance the perturbative transverse energy flux. Due to the x -component of the first-order perturbative EM power flux density including the effect of HFGWs, it becomes our concern signal and its directly observable effect should be the corresponding photon number (i.e., perturbative photon flux $N_x^{(1)}$ (PPFs)). The density of PPFs is

$$n_x^{(1)} = \frac{1}{\hbar\omega_e} \left\langle \frac{1}{\mu_0} (\tilde{E}_y^{(1)*} \cdot \tilde{B}_z^{(0)}) \right\rangle, \quad (12)$$

where $\langle \rangle$ denotes the average value over a period. And

$$N_x^{(1)} = \int_z \int_y n_x^{(1)} dydz. \quad (13)$$

Then considering the earth rotation, all the observable physical effect should be averaged by the inclination angle θ . Moreover for the Relic HFGWs, the PPFs also need to be averaged by δ since its stochastic initial phase. Then they can be distinguished as

Relic HFGWs:

$$N_x^{(1)} = \frac{1}{2\pi^2} \int_0^{2\pi} d\delta \int_{-\frac{\pi}{2}}^{\frac{\pi}{2}} d\theta \int_z \int_y n_x^{(1)} dydz. \quad (14)$$

HFGWs from braneworld:

$$N_x^{(1)} = \frac{1}{\pi} \int_{-\frac{\pi}{2}}^{\frac{\pi}{2}} d\theta \int_z \int_y n_x^{(1)} dydz. \quad (15)$$

According to the Eq.(8),(14) and (15), the electromagnetic response of the Relic HFGWs and the HFGWs from the braneworld would be determined. As an example, Fig.2 illuminates the properties of PPFs from Relic HFGWs and braneworld HFGWs, which reveals (1) for each kind of HFGWs, the PPFs behaves as an even function on the x axis, and the maximum PPFs always appear at $x = 0$ plane with $z > 0$. Meanwhile the peak value of signal will decay along the direction of GB propagation. (2) Since the amplitude of braneworld HFGWs exceeds to the Relic HFGWs' amplitude 4 orders, the PPFs from braneworld HFGWs always stronger the same order than the results of Relic HFGWs. Therefore, the PPFs on $x = 0$ plane toward to positive z direction is our ideal detection signal.

III. NOISE ANALYSIS

A. Background Noise

As mentioned above, in the response system the GB in microwave is used as supplying a longitudinal magnetic field component $\tilde{B}_z^{(0)}$, which provides the necessary resources to produce the signal (PPFs). However it also causes the major noise of the system called as the background photon fluxes (BPFs). That can be deduced as

$$n_x^{(0)} = \frac{1}{\hbar\omega_e} \left\langle \frac{1}{\mu_0} (\tilde{E}_y^{(0)*} \cdot \tilde{B}_z^{(0)}) \right\rangle, \quad (16)$$

and

$$N_x^{(0)} = \int_z \int_y n_x^{(0)} dydz. \quad (17)$$

Comparing Eq.(16),(17) with Eq.(12),(13), it can be found that the BPFs come from the GB's electric y -component $\tilde{E}_y^{(0)}$ coupling to its longitudinal magnetic component $\tilde{B}_z^{(0)}$. It is worthy to emphasize that the difference between the PPFs and BPFs is the different coupling electric components. Even though due to the $\tilde{E}_y^{(0)} \gg \tilde{E}_y^{(1)}$ the PPFs

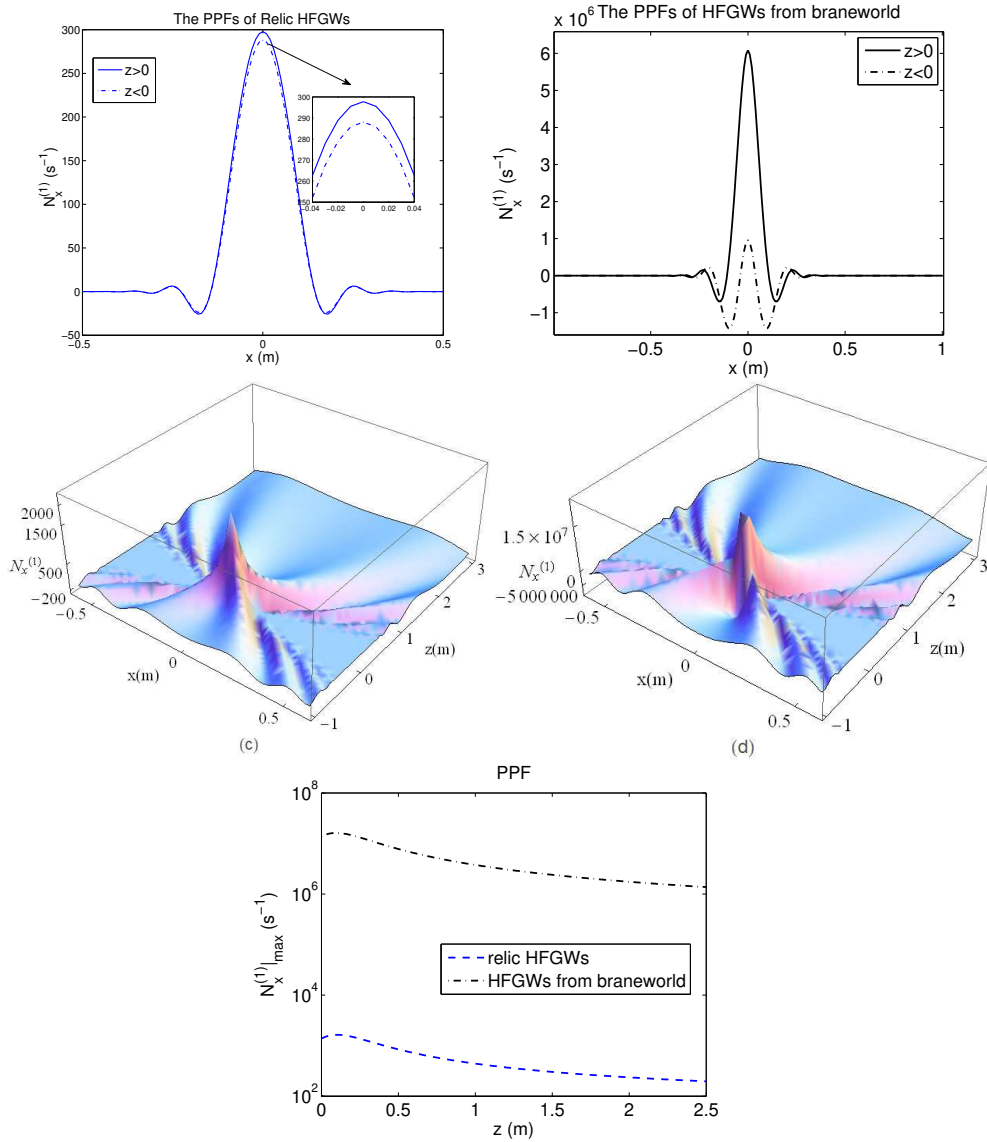


FIG. 2: (a) The perturbative photon fluxes of relic HFGWs, assuming $A_{\oplus} = A_{\otimes} = 10^{-30}$; (b) The perturbative photon fluxes of HFGWs from braneworld with $A_{\oplus} = A_{\otimes} = 10^{-26}$ and setting $\delta = 1.32\pi$; (c) The 3D plot of the corresponding transverse perturbation photon fluxes $N_x^{(1)}$ produced by the Relic HFGWs; (d) The 3D plot of the corresponding transverse perturbation photon fluxes $N_x^{(1)}$ from braneworld HFGWs. (e) The maximum value of PPFs varying with z axis. Here $\hat{B}_y^{(0)} = 6T, P = 10W, W_0 = 5\text{cm}$.

are significantly submerged by the BPFs in most areas, on some specific planes the PPFs would exceed to the BPFs. Fig.3 gives the numerical results of the BPFs, and contrasting to the PPFs (cf. Fig.2) it can be found the maximum value of the BPFs is much larger than the peak value of the PPFs, but their distributions are completely different. On one hand, the BPFs is odd symmetry for $x = 0$ and when $z > 0$ they propagate depart from $x = 0$ (outgoing), while when $z < 0$ they face to each other (imploding), and $N_x^{(0)}|_{x=0} = 0$. On the other hand, the PPFs is even symmetry for $x = 0$ and the maximum value when $z > 0$ exceeds the one in the $z < 0$ case, so that the positive z direction is our expected detection area. The most important thing is that on the $x = 0$ plane, the PPFs reach to the maximum value while the BPFs vanish, in other words, on the $x = 0$ plane the signal-to-noise ratio can reach considerable value so that in this place the detection will be realized in a suitable way. In practice this optimal plane is extremely narrow, so a new material or equipment which can play a focusable role in the system is very urgent. Fortunately, a new type of fractal membranes can satisfy such requirement that will be discussed below.

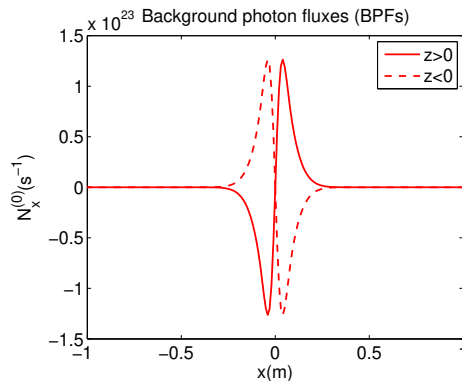


FIG. 3: The transverse background photon fluxes. Here assuming $P = 10\text{W}$, $W_0 = 5\text{cm}$. Note: the minus value means the photon flux propagate along the negative direction of the x -axis.

B. Shot Noise

As a general microwave detector, our electromagnetic response scheme contains a large number of photons and electrons. So we pay attention to the noise generated from particles statistical fluctuations (i.e., shot noise). For shot noise, the dark-background shot noise generated from the GB and signal shot noise from signal photon fluxes should be evaluated simultaneously.

In this paper, the dark background shot noise is proportional to the square root of the number of BPF, which has the form as [27]

$$P_{nd} = h\nu_e \sqrt{N_x^{(0)}/\Delta t}; \quad (18)$$

Meanwhile the signal shot noise from the signal can not be subject to elimination, which has the similar form as the dark background shot noise,

$$P_{ns} = h\nu_e \sqrt{N_x^{(1)}/\Delta t}. \quad (19)$$

Where Δt is the sample or accumulation time. The above results are calculated with $\Delta t = 1\text{s}$, then the dark background shot noise and signal shot noise can be given in Fig.4. It can be found that the power of the background shot noise is overwhelming, resulting in the SNR greatly being reduced. According to the requirement of signal detection as following equation, the detection sensitivity in such case can be estimated as follows,

$$|N_x^{(1)}|^2 \Delta t_{total} \geq |N_x^{noise}|, \quad (20)$$

where Δt_{total} is the requisite total signal accumulation time, and N_x^{noise} includes the noisy photons mainly from BPF and shot noise. If we restrict the $\Delta t_{total} = 3\text{monthes}$, and assume the most conservative estimation (i.e., the major background noise (BPFs) with maximum value $\sim 6 \times 10^{22}\text{s}^{-1}$, the dimensionless amplitude of the HFGWs should reach up to $A_{\oplus}(A_{\otimes}) \sim 10^{-26}$. That means without any other additional equipment, the HFGWs from braneworld might be detectable in this scheme. However for the relic HFGWs, the system need to employ some instrument having signal focusing performance e.g. the fractal membranes[28]-[30].

In order to weaken the background shot noise, it is necessary to reduce the BPFs. That is why we use the fractal membranes (FM) with their plane overlap the $x = 0$ plane where $N_x^{(0)} = 0$ (cf.fig.1), which can keep the maximum strength of the PPFs ($N_x^{(1)}$) invariant within certain distance[28],[29]. As our previous works [19],[21], it is considered to be that after $N_x^{(1)}$ is transmitted, it also keeps its 90 percent strength in 1 meter. Table 1 lists the BPFs and PPFs after using the FM and Fig.5 shows the total shot noise and signal power comparison. In the region of $60\text{cm} \leq x \leq 70\text{cm}$, the SNR would be larger than 1. So it is reasonable to choose this region as our detection district. Then we will estimate the standard quantum limit in such area.

C. The Standard Quantum Limit (SQL) Estimation

For all measurement systems, there is a kind of noise produced by the Heisenberg uncertainty principle [31], as a result the sensitivity would be limited. That is well known as "standard quantum limit (SQL)". In this section,

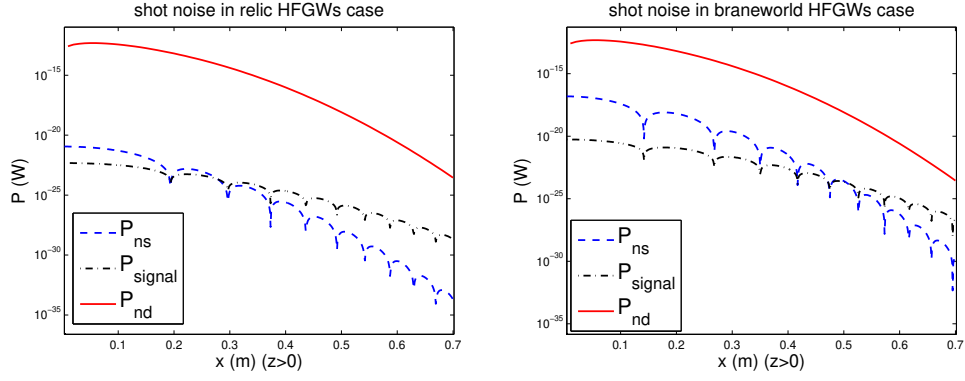


FIG. 4: The dark background shot noise and signal shot noise versus signal power on transverse direction. Here setting $\theta = 0$, $\hat{B}_y^{(0)} = 6T$, $P = 10W$, $\delta = 1.32\pi$, $W_0 = 9\text{cm}$.

TABLE I: Comparison of BPFs ($|N_x^{(0)}|$) and PPFs ($|N_x^{(1)}|_{\text{FM}}$) with fractal membrane in the x-direction. Note beyond 0.7m the photon number of the BPFs is less than 1, so the area can be neglected.

$x(m)$	0	0.05	0.61	0.66	0.70
$ N_x^{(0)} (s^{-1})$	0	5.8×10^{22}	4.6×10^5	603	2
relic : $ N_x^{(1)} _{\text{FM}}(s^{-1})$	568.40	565.60	533.70	530.90	528.60
braneworld : $ N_x^{(1)} _{\text{FM}}(s^{-1})$	7.80×10^6	7.76×10^6	7.32×10^6	7.28×10^6	7.25×10^6

considering the energy contained within the detector and various possible sources having contribution to Quality Factor Q , the SQL for the relic HFGWs and the braneworld HFGWs are estimated.

Following the SQL for GWs detectors calculated by Grishchuk, the SQL of a stochastic GW is given by [32],

$$h_{\text{det}} = \sqrt{\frac{1}{Q}} \sqrt{\hbar \omega_g / \varepsilon}, \quad (21)$$

and for a coherent GW, it should be

$$h_{\text{det}} = \frac{1}{Q} \sqrt{\hbar \omega_g / \varepsilon}, \quad (22)$$

where ε is the effective energy contained in the system summed over the detection averaging time. According to the description for our EM response system, the Q , which can be understood as the selectivity of the signal over noise,

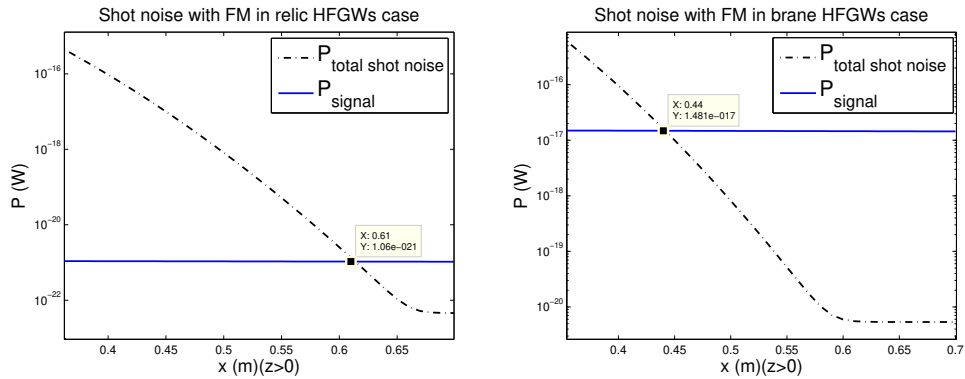


FIG. 5: The total shot noise and signal power on transverse direction.

would be discussed as follows,

$$Q_{\text{total}} = Q_{\text{FM}} Q_{\text{solidangle}} Q_{\text{t}}, \quad (23)$$

where Q_{FM} arising from the fractal membranes. From Table 1 and Fig. 2, it can be given as

$$Q_{\text{FM}} = \text{SNR}_{\text{FM}}/\text{SNR}|_{r=70\text{cm}} = \begin{cases} 1.76 \times 10^{14} & \text{relic HFGWs} \\ 2.42 \times 10^7 & \text{braneworld HFGWs} \end{cases}, \quad (24)$$

and Q_{t} is the temporal quality factor in the system from averaging the signal over time (typically the averaging time can be chosen as $\Delta t = 10^3\text{s}$), so $Q_{\text{t}} = \omega_g \Delta t / 2\pi = 3 \times 10^{12}$. Another quality factor $Q_{\text{solidangle}}$ is a contribution in angular space, the effective antenna gain should be roughly estimated to be $Q_{\text{solidangle}} = 6.3 \times 10^4$ [32].

Here the background EM fields consisting of a static magnetic field $\hat{B}_y^{(0)}$ and GB store a huge energy, so that the energy density stored in the system is

$$\varepsilon = P \cdot \Delta t + \frac{(\hat{B}_y^{(0)})^2}{2\mu_0} = 1.4 \times 10^7. \quad (25)$$

For the relic HFGWs, the corresponding SQL can be evaluated according to Eq.(21) yielding $h_{\text{det}} = 6.46 \times 10^{-32}$, while for the HFGWs from braneworld the SQL should become much lower than $h_{\text{det}} \sim 10^{-32}$ (cf. Eq.(22)). Therefore the SQL results imply that our EM response system would not be limited by quantum noise, versus the predicted values of the dimensionless amplitudes of the relic HFGWs $h \sim 10^{-30}$ and the HFGWs from braneworld $h \sim 10^{-26}$.

IV. PARAMETRIC ANALYSIS

In experiment, it is always expected to obtain the optimal effect. Thus how to select parameters is another issue for us, following the principle of maximum SNR we discuss the optimal system parameters such as, waist of GB (W_0), bandwidth and resonance frequency (ν).

Firstly, the waist of GB (W_0) plays significant role on the transverse PPFs production. Fig.6 describes the background photon fluxes (BPFs) and the perturbative photon fluxes (PPFs) varying different waist of GB. That indicates the larger waist of GB (W_0) can result in stronger signal energy, and weaken the strength of the BPF considered to be the major background noise (the background shot noise would be reduced simultaneously). Here the wavelength of the HFGWs is $\lambda = 10\text{cm}$ corresponding to $\nu = 3\text{GHz}$, so the upper limit of the waist should be 10cm. Therefore, for the given conditions ($\nu = 3\text{GHz}$, $\hat{B}_y^{(0)} = 6\text{T}$, $P = 10\text{W}$), the waist $W_0 = 9\text{cm}$ could achieve the highest SNR.

Secondly, the bandwidth of the laser is inevitable. Now about the effect of bandwidth in our system is also taken into our concern. According to Eq.(12), the PPFs should be proportional to $\langle \cos(k_g z - \omega_g t) \cos(k_e z - \omega_e t + \delta) \rangle$, which can be separated into the following two intergrations,

$$\begin{aligned} \tilde{n}_x^{(1)} \propto & (\omega_g - \omega_e) \int_0^{\frac{2\pi}{\omega_g - \omega_e}} \cos((k_g - k_e)z - (\omega_g - \omega_e)t - \delta_0) dt + \\ & (\omega_g + \omega_e) \int_0^{\frac{2\pi}{\omega_g + \omega_e}} \cos((k_g + k_e)z - (\omega_g + \omega_e)t + \delta_0) dt. \end{aligned} \quad (26)$$

So when $\omega_g = \omega_e$, $\tilde{n}_x^{(1)} \propto \cos\delta$, while $\omega_g \neq \omega_e$, $\tilde{n}_x^{(1)} = 0$. In other words, the components of GWs and GB with different frequency can not resonate to each other. That means the frequency bandwidth would not influence the original signal. Finally, it should be clarified that theoretically the frequency of the HFGWs can range from 10^8Hz to 10^{10}Hz for the relic HFGWs and even reach up to 10^{14}Hz in braneworld case[10]. Thus the resonance frequency ν should be variable. The corresponding results in Fig.7 illuminates that with the frequency increase even although the maximum values of PPFs will decrease slightly, the directive property of PPFs becomes much better (i.e. the propagation direction of signal energy fluxes tends to be non-oscillating state). So it is meaningful to define the transverse area around $x = 0$ plane with positive PPFs as effective width D_{eff} . Then Fig.7(c) has shown the general relationship between the effective width and frequency. It can be found with the frequency growth the effective width will become wider, in other words, in the higher frequency band the effective energy fluxes can be enhanced greatly. Furthermore it is worthy to emphasize that with the frequency increase the BPFs will decrease more quickly than the PPFs (cf. Table 2), which means the SNR will be further improved in higher frequency band.

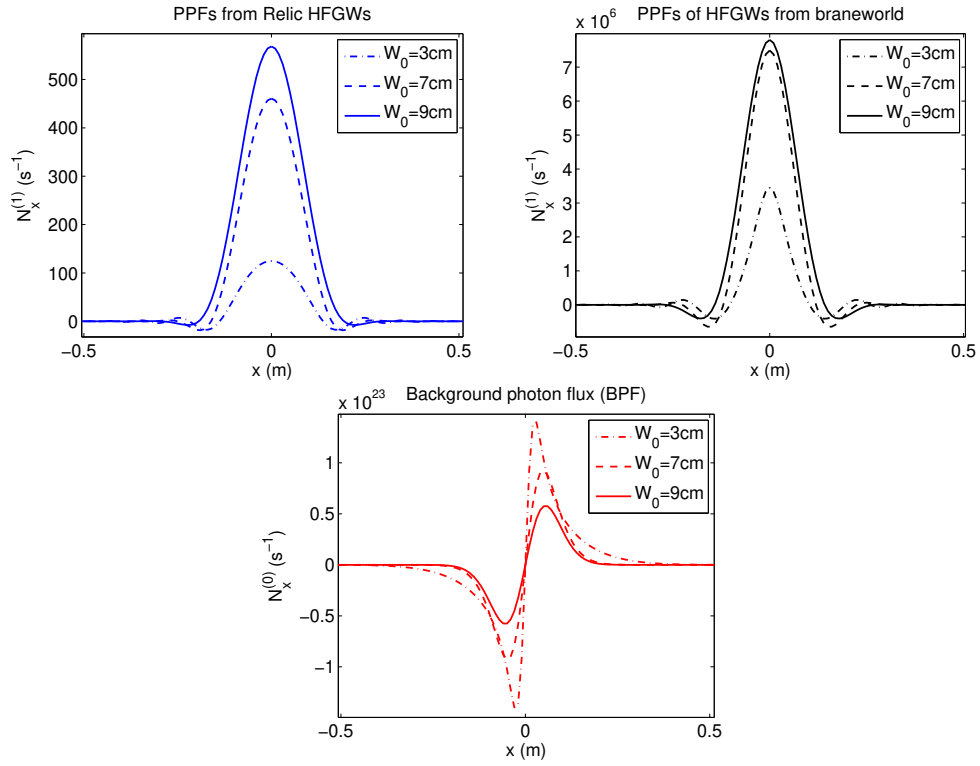


FIG. 6: The effect of the GB waist on the transverse background photon fluxes (BPFs) and perturbation photon fluxes (PPFs). Here $\nu = 3\text{GHz}$, $\hat{B}_y^{(0)} = 6\text{T}$, $P = 10\text{W}$, $z > 0$ and for braneworld HFGWs supposing $\delta = 1.32\pi$.

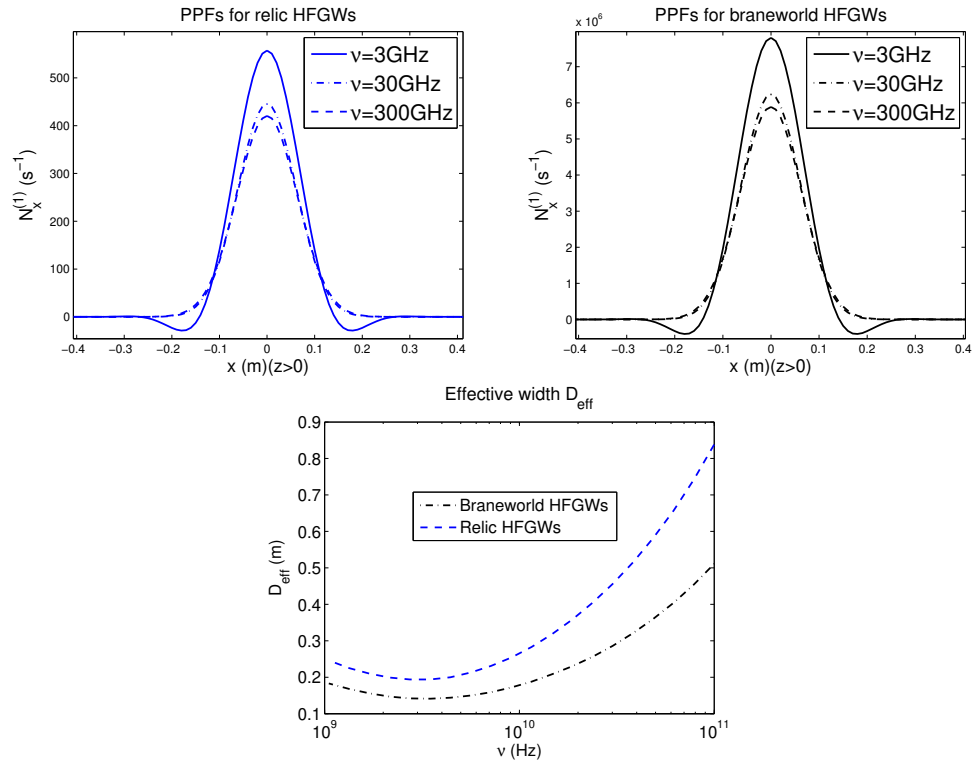


FIG. 7: The effect of frequency. Here choosing the waist as the optimal value $W_0 = 9\text{cm}$.

TABLE II: The maximum value of the PPFs ($N_x^{(1)}|_{\max}$) and BPFs ($N_x^{(0)}|_{\max}$) varying with some typical frequencies. For relic HFGWs we suppose $A_{\oplus} = A_{\otimes} = 10^{-30}$. Although the dimensionless amplitude h varies with frequency in ordinary inflation model, it can be held at this order of magnitude through choosing different inflation parameters [17]. For braneworld HFGWs, assuming $A_{\oplus} = A_{\otimes} = 10^{-26}$.

$\nu(\text{GHz})$	$N_x^{(1)} _{\max} (s^{-1})$		$N_x^{(0)} _{\max} (s^{-1})$
	relic HFGWs	braneworld HFGWs	
3	557.30	7.80×10^6	1.40×10^{23}
30	445.50	6.24×10^6	5.03×10^{21}
300	420.40	5.89×10^6	7.14×10^{18}

V. CONCLUSION

. Based on the electromagnetic response system of HFGWs, we discussed the EM effects from the relic HFGWs and the braneworld HFGWs contrastly, and found the optimal parameters to improve sensitivity. The main remarks of this paper can be classified as follows,

(1) For the relic HFGWs (around GHz band) predicted by QIM may store a large amount of energy, the scheme discussed in this paper can be considered as a hopeful candidate for such GWs detection. Under the typical conditions of resonant response and consider the isotropic property of the relic GWs, the first-order transverse perturbative photon fluxes (PPFs) would be expected to be $\sim 3 \times 10^2 s^{-1}$, This result is much better than our previous work [21] because the longitudinal background magnetic component is set to be the standard Gaussian form. Meanwhile as a coherent GWs source, the HFGWs from braneworld would generate much stronger PPFs $\sim 6 \times 10^6 s^{-1}$ due to its quite larger dimensionless amplitude h . So if the braneworld scenarios is correct, our EM response system would be much more hopeful to capture the GWs from extra dimensional braneworld.

(2) Although the BPFs exceed to the PPFs in some areas, the $x = 0$ plane is always chosen to be the ideal detection place since there is no BPFs. Furthermore such advantage of $x = 0$ plane would be maintained in a certain distance using a focusing material (such as FM in this paper), and the signal to noise ratio (SNR) can be greatly improved. Especially the transverse detection range of the relic HFGWs would spread from 61cm to 70cm and of the braneworld HFGWs would be wider that is $44\text{cm} < x < 70\text{cm}$. Certainly there must be some other focusing equipment rather than FM, this will be taken into our consideration in the future work. The SQL analysis indicates that no matter for the relic or braneworld HFGWs, the limit of your detection is not from quantum noise.

(3) The system parameters play very important roles in signal detection. Focusing on the GB waist, frequency bandwidth and response frequency, we analyzed their effect on the SNR, and found the optimal waist $W_0 = 9\text{cm}$ under the typical condition. Additionally in the possible HFGWs' frequency band, the higher response frequency would result in better detection effect (higher SNR and larger effective width for energy fluxes accumulation). Those are independent from frequency bandwidth.

Acknowledgements

We would like to express my gratitude to Professor Fangyu Li for his great help. This work is supported by FAPESP No. 2012/08934-0, National Natural Science Foundation of China No. 11205254, No. 11178018 and No. 11375279, and the Natural Science Foundation Project of CQ CSTC 2011BB0052, and the Fundamental Research Funds for the Central Universities CQDXWL-2013-010 and CDJRC10300003.

-
- [1] A. Abramovici *et al.*, *Science* **256** 325 (1992).
[2] R. Caldwell, M. Kamionkowski, and L. Madley, *Phys. Rev. D* **59** 027101 (1999).
[3] Y. Jafry, J. Corneliss, and R. Reinhard, *ESA Bull* **18** 219 (1994).
[4] P. A. R. Ade *et al.*, *Phys. Rev. Lett.* **112** 241101 (2014).

- [5] Planck collaboration, arXiv: 1303.5062.
- [6] Planck collaboration, arXiv: 1303.5076.
- [7] Planck collaboration, arXiv: 1303.5083.
- [8] Planck collaboration, *A and A* **564** A45 (2014).
- [9] S. S. Seahra, C. Clarkson, and R. Maartens, *Phys. Rev. Lett.* **94** 121302 (2005).
- [10] C. Clarkson and S. S. Seahra, *Classical Quantum Gravity* **24** F33 (2007).
- [11] M. Giovannini, *Phys. Rev. D* **60** 123511 (1999).
- [12] M. Giovannini, *Class. Quantum Grav.* **16** 2905 (1999).
- [13] A. Riazuelo, J. P. Uzan, *Phys. Rev. D* **62** 083506 (2000).
- [14] P. Peebles and A. Vilenkin, *Phys. Rev. D* **59** 063505 (1999).
- [15] J. P. Ostriker and P. J. Sternhardt, *Sci. Am. Int. Ed.* **284** 46 (2001).
- [16] Y. Zhang, X. Z. Er, T. Y. Xia, W. Zhao and H.X. Miao, *Class. Quantum Grav.* **23** 3783 (2006).
- [17] Y. Zhang, H. X. Maio, *Phys. Rev. D* **75** 104009 (2007).
- [18] F. Y. Li *et al.*, *Phys. Rev. D* **80** 064013 (2009).
- [19] F. Y. Li *et al.*, *Eur. Phys. J. C* **56** 407 (2008).
- [20] F. Y. Li, M. X. Tang, D. P. Shi, *Phys. Rev. D* **67** 104008 (2003).
- [21] J. Li *et al.*, *Gen. Relativ. Gravit.* **43** (2011) 2209-2222.
- [22] S. S. Seahra, *Phys. Rev. D* **72** 066002 (2005).
- [23] H. Wen, F. Y. Li, and Z. Y. Fang, *Phys. Rev. D* **89** 104025 (2014).
- [24] W. K. De Logi, A. R. Mickelson, *Phys. Rev. D* **16** 2915 (1977).
- [25] D. Boccaletti *et al.*, *Nuovo Cim. B* **70** 129 (1970).
- [26] A. Yariv, *Quantum Electronics* 2nd ed.(Wiley, NewYork, 1975).
- [27] R. Clive Woods *et al.*, *Journal of Modern Physics* **2** 498-518 (2011).
- [28] W. J. Wen *et al.*, *Phys. Rev. Lett.* **89** 223901 (2002).
- [29] L. Zhou *et al.*, *Appl. Phys. Lett.* **82** 1012 (2003).
- [30] B. Hou *et al.*, *Opt. Express* **13** 9149 (2005).
- [31] T. J. Kippenberg and K. J. Vahala, *Science* **321** No. 5893, 2008, pp. 1172-1176.
- [32] G. V. Stephenson, *Proceedings of American Institute of Physics Conference*, Springer-Verlag, New York, Vol. 1103, 2009, pp. 542-547.